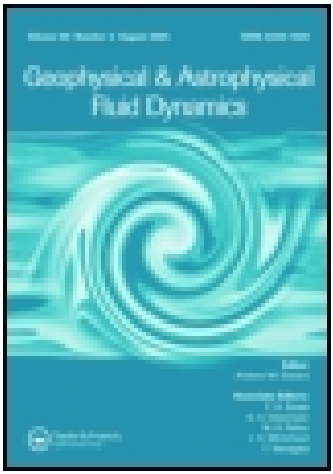

Geophysical & Astrophysical Fluid Dynamics

Publication details, including instructions for authors and subscription information:
http://www.tandfonline.com/loi/ggaf20

On the onset of convection in rotating spherical shells

K.-K. Zhang [a] & F. H. Busse [a b]

[a] University of Bayreuth , 8580, Bayreuth, West Germany

[b] Institute of Geophysics and Planetary Physics, University of California at Los Angeles , CA, 90024, USA

Published online: 18 Aug 2006.

To cite this article: K.-K. Zhang & F. H. Busse (1987) On the onset of convection in rotating spherical shells, Geophysical & Astrophysical Fluid Dynamics, 39:3, 119-147

To link to this article: http://dx.doi.org/10.1080/03091928708208809

Geophys. Astrophys. Fluid Dynamics, Vol. 39, 119–147
Photocopying permitted by license only

Printed in Great Britain

On the Onset of Convection in Rotating Spherical Shells

K.-K. ZHANG and F. H. BUSSE

University of Bayreuth, 8580 Bayreuth, West Germany, and Institute of Geophysics and Planetary Physics, University of California at Los Angeles, CA 90024, USA

(*Received December 29, 1986*)

The linear problem of the onset of convection in rotating spherical shells is analysed numerically in dependence on the Prandtl number. The radius ratio $\eta = r_i/r_0$ of the inner and outer radii is generally assumed to be 0.4. But other values of η are also considered. The goal of the analysis has been the clarification of the transition between modes drifting in the retrograde azimuthal direction in the low Taylor number regime and modes traveling in the prograde direction at high Taylor numbers. It is shown that for a given value m of the azimuthal wavenumber a single mode describes the onset of convection of fluids of moderate or high Prandtl number. At low Prandtl numbers, however, three different modes for a given m may describe the onset of convection in dependence on the Taylor number. The characteristic properties of the modes are described and the singularities leading to the separation with decreasing Prandtl number are elucidated. Related results for the problem of finite amplitude convection are also reported.

KEY WORDS: Thermal convection, rotating spheres.

1. INTRODUCTION

The problem of convection in rotating spherical fluid shells subject to spherically symmetric gravity fields is of basic importance for the understanding of the dynamics of planetary and stellar atmospheres. Considerable progress has been made in solving linear as well as nonlinear aspects of this problem, but extensive blank areas in the

parameter space of this problem still exist. The large number of parameters that describe the problem is in part responsible for its insufficient exploration. While the case of horizontal plane layer rotating about a vertical axis is typically characterized by three parameters, namely the Rayleigh number, the Prandtl number and the Taylor number, several new parameters such as the radius ratio, the mode of heating and the variation of gravity must be specified for the rotating spherical shell. The various possibilities for the distributions of heat sources and gravity seem to have relatively little influence on the onset and form of convection as is evident from the treatment of the non-rotating case (Chandrasekhar, 1961). It thus seems that the case of a homogeneously heated sphere with a gravity force varying linearly with radius can be regarded as the standard model. This simplification of the analysis will be adopted in this paper. The only disadvantage of this assumption is that the ratio between internally generated heat flux and the heat flux applied at the inner boundary will vary with the radius ratio η of the fluid shell. Because in planetary and stellar applications only the super-adiabatic part of the temperature gradient enters the Rayleigh number, there is no clear preference for any particular kind of model, and the standard model adopted here offers the advantage of mathematical simplicity.

The emphasis of present study of the onset of convection in rotating spherical shells is on the effect of the Prandtl number P. Because of the wave-like drift of the preferred modes of convection, the Prandtl number enters the problem already in its linear form in contrast to the Prandtl number independent onset in the limit of vanishing rotation. Previous numerical computations (Gilmann 1975, Cuong 1979) of the critical parameters for the onset of convection have almost exclusively been restricted to the case $P=1$. The dependence of the critical Rayleigh number R_c on the Taylor number shown by Cuong (1979) exhibits some unusual bends and the corresponding frequency ω_c also did not show the expected smooth variation with Taylor number. In this paper this curious feature is investigated in more detail and it is shown that for $P \gtrsim 1$ the dependence of R_c and ω_c on the Taylor number T for a given value m of the azimuthal wavenumber is continuously differentiable, but below a certain value $P(m)$ of the Prandtl number kinks appear in the $R_c(T)$ and $\omega_c(T)$ relationships because one mode is replaced by another one with the same value of m.

Two different switchovers of this kind have been identified in the present analysis. The switchover at low Taylor numbers is connected with the change from a retrograde drift to a prograde drift with respect to the sense of rotation. The second switchover occurring at high Taylor numbers is connected with the development of a loop in the Rayleigh–Taylor number relationship. In the asymptotic regime of large Taylor numbers the dispersion relation approaches that expected for thermal Rossby waves for which approximate analytic expressions can be obtained (Busse, 1970). Since asymptotic expressions are independent of the ratio η between the radius of inner and outer boundaries as long as $\eta \lesssim 0.5$, most computations have been done for $\eta = 0.4$. This case also seems to be most relevant to the earth's core which exhibits a radius ratio near this value.

The mathematical method is outlined in Section 2. Results for moderate to high Prandtl numbers are discussed in Section 3. The low Prandtl number regime is analysed in Section 4. Some nonlinear results are described in Section 5 and concluding remarks are added in Section 6.

2. MATHEMATICAL FORMULATION OF THE ANALYSIS

We consider a spherical fluid shell with outer radius r_0 and inner radius ηr_0 as shown in Figure 1. A uniform distribution of heat sources inside the radius r_0 give rise to the static temperature distribution

$$T_s = T_0 - \beta r^2/2 \tag{2.1}$$

The gravity distribution throughout the fluid shell is given by

$$\mathbf{g} = -\gamma \mathbf{r} \tag{2.2}$$

where $\mathbf{r}$ is the position vector with respect to the center of the sphere. The sphere is rotating with the angular velocity Ω about an axis described by the unit vector $\mathbf{k}$. Using the thickness of the shell, $d \equiv r_0(1-\eta)$, as length scale, d^2/ν as time scale, where ν is the kinematic viscosity, and $\beta d^2 \nu/\kappa$ as scale of the temperature we arrive at the following non-dimensional forms of the equations of motion and the heat equation,

$$\frac{\partial u}{\partial t} + \mathbf{u} \cdot \nabla \mathbf{u} + \tau \mathbf{k} \times \mathbf{u} = -\nabla \pi + R \mathbf{r} \Theta + \nabla^2 \mathbf{u} \tag{2.3a}$$

$$\nabla \cdot \mathbf{u} = \mathbf{0} \tag{2.3b}$$

$$P\left(\frac{\partial}{\partial t} + \mathbf{u} \cdot \nabla\right)\Theta = \mathbf{u} \cdot \mathbf{r} + \nabla^2 \Theta \tag{2.3c}$$

The Boussinesq approximation has been assumed and the dimensionless deviation Θ of the temperature from the static distribution (2.1) has been introduced as a new variable. The parameters of the problem are represented by the Rayleigh number R, the Taylor number, $T \equiv \tau^2$, and the Prandtl number P,

$$R = \frac{\alpha\gamma\beta d^6}{\nu\kappa}, \; T^{1/2} = \tau = 2\Omega d^2/\nu, \quad P = \frac{\nu}{\kappa} \tag{2.4}$$

where α is the coefficient of thermal expansion and κ is the thermal diffusivity. It is convenient to eliminate the need for the equation of continuity (2.3b) by the introduction of the general representation for the solenoidal vector field $\mathbf{u}$,

$$\mathbf{u} = \nabla \times (\nabla \times \mathbf{r}v) + \nabla \times \mathbf{r}w \tag{2.5}$$

The scalar functions v, w are uniquely defined if their average over any concentric spherical surface vanishes. By multiplying the curl and the curlcurl of Eq. (2.3a) by $\mathbf{r}$ we obtain two equations for v and w,

$$\left[\left(\nabla^2 - \frac{\partial}{\partial t}\right)L_2 + \tau \mathbf{k} \times \mathbf{r} \cdot \nabla\right] w - \tau Q v = \mathbf{r} \cdot \nabla \times (\mathbf{u} \cdot \nabla \mathbf{u}) \tag{2.6a}$$

$$\left[\left(\nabla^2 - \frac{\partial}{\partial t}\right)L_2 + \tau \mathbf{k} \times \mathbf{r} \cdot \nabla\right] \nabla^2 v + \tau Q w - R L_2 \Theta = -\mathbf{r} \cdot \nabla \times (\nabla \times (\mathbf{u} \cdot \nabla \mathbf{u})) \tag{2.6b}$$

where L_2 represents the negative Laplacian on the unit sphere and the operator Q can be written in the form

$$Q \equiv \mathbf{k} \cdot \nabla - \tfrac{1}{2}(L_2 \mathbf{k} \cdot \nabla + \mathbf{k} \cdot \nabla L_2) \tag{2.7}$$

For the numerical analysis of Eqs. (2.6), (2.3c) we introduce a spherical system of coordinates (r, θ, ϕ) with the polar axis in the direction of $\mathbf{k}$. In these coordinates the operator L_2 is given by

$$L_2 = -\frac{1}{\sin\theta}\frac{\partial}{\partial\theta}\left(\sin\theta\frac{\partial}{\partial\theta}\right) - \frac{1}{\sin^2\theta}\frac{\partial^2}{\partial\phi^2}$$

We assume stress-free boundary conditions at the boundaries of the shell and require that the temperature is fixed at those boundaries,

$$v = \frac{\partial^2}{\partial r^2}v = \frac{\partial}{\partial r}\left(\frac{w}{r}\right) = \Theta = 0 \quad \text{at} \quad r = \eta/(1-\eta)$$

$$\text{and} \quad r = 1/(1-\eta) \tag{2.8}$$

Because of the formation of Ekman layers at rigid boundaries, the latter are more difficult to deal with in computational schemes. It is known (Roberts, 1965), however, that in the limit of large Taylor number the differences between the solutions induced by the difference in the boundary conditions become small except in the Ekman layers.

In order to solve Eqs. (2.6) and (2.3c) by the Galerkin method, we expand v, w and Θ in terms of functions satisfying the boundary conditions (2.8),

$$v = \sum_{\nu,n,l} a_{\nu nl}\exp\{i\nu(m\phi+\omega t)\}P_l^{|\nu|m}(\cos\theta)$$

$$\times \sin n\pi[r-\eta(1-\eta)^{-1}] \tag{2.9a}$$

$$w = r\sum_{\nu,n,l} C_{\nu nl}\exp\{i\nu(m\phi+\omega t)\}P_l^{|\nu|m}(\cos\theta)$$

$$\cos(n-1)\pi[r-\eta(1-\eta)^{-1}] \tag{2.9b}$$

$$\theta = \sum_{\nu,n,l} b_{\nu nl}\exp\{i\nu(m\phi+\omega t)\}P_l^{|\nu|m}(\cos\theta)$$

$$\sin n\pi[r-\eta(1-\eta)^{-1}] \tag{2.9c}$$

where the index n runs through all positive integers while the indices l and $\hat{l}$ run through $|v|m, |v|m+2, |v|m+4, \ldots$, and $|v|m+1, |v|m+3, \ldots$, respectively, in the case of solutions which are symmetric with respect to the equatorial plane. The role of l and $\hat{l}$ is interchanged for solutions which are antisymmetric. $P_l^\mu(\cos\theta)$ is the associated Legendre polynomial which we shall use in the normalized form such that $[P_l^\mu]^2$ averaged over the unit sphere yields unity,

$$P_l^\mu(x) \equiv \left[\frac{(l-\mu)!(2l+1)}{(l+\mu)!}\right]^{1/2} 2^{-l}(l!)^{-1}(-1)^\mu \times (1-x^2)^{\mu/2}\frac{d^{l+\mu}}{dx^{l+\mu}}(x^2-1)^l. \tag{2.10}$$

When we consider the linear problem, the index v is set equal to unity as we shall do for most of the following analysis. In the nonlinear case v runs through all integers and the complex coefficients obey the relationships

$$a_{-vnl} = a_{vnl}^*, \; b_{-vnl}^* = b_{vnl}, \; c_{-vn\hat{l}} = c_{vn\hat{l}}^* \tag{2.11}$$

where the star indicates the complex conjugate. After inserting expressions (2.9) into Eqs. (2.6) and (2.3c), multiplying these equations by the complex conjugates of the expansion functions used in expressions (2.9) and averaging the equations over the spherical shell we obtain a system of algebraic equations for the coefficients $a_{vnl}, c_{vn\hat{l}}, b_{vnl}$. In order to get an approximate numerical solution for this infinite system we must truncate the number of coefficients and equations by introducing a truncation procedure. Usually we shall neglect all coefficients and corresponding equations whenever

$$2n + l - |v|m + 2|v| > 2N_T + 3 \tag{2.12}$$

where N_T is a positive integer chosen to equal to 3, 4, 5 or 6, depending on the requirements for accuracy. Inequality (2.12) also holds for $\hat{l}$ instead of l.

Most of the following analysis will be focussed on the linear problem in which terms corresponding to the right hand side of Eqs. (2.6) and (2.3c) are neglected. The linear equations for the coefficients

Table I Gives some examples for the critical Rayleigh numbers and corresponding drift rates, $c=\omega/m$ which have been obtained at the Taylor number $T=10^6$ for different values of the Prandtl number and of the truncation parameter N_T

N_T \ P,m	$m=4$ $P=0.01$	$m=6$ $P=0.1$	$m=6$ $P=1.0$	$m=6$ $P=10.0$
$N_T=3$	$R_c=1901.8$ $c=-113.4$	$R_c=4382.4$ $c=17.35$	$R_c=12367$ $c=5.981$	$R_c=20575$ $c=0.7639$
$N_T=4$	$R_c=1887.1$ $c=-113.5$	$R_c=4408.0$ $c=17.23$	$R_c=13165$ $c=5.688$	$R_c=20121.6$ $c=0.677$
$N_T=5$	$R_c=1930.3$ $c=-113.5$	$R_c=4432.1$ $c=17.15$	$R_c=13067$ $c=5.704$	$R_c=20186.7$ $c=0.685$
$N_T=6$	$R_c=1935.1$ $c=-113.4$	$R_c=4426.5$ $c=17.14$	$R_c=13182$ $c=5.698$	$R_c=20204$ $c=0.6772$

$a_{vnl}, b_{vnl}, c_{vnl}$ contain ω as eigenvalue. For given values of m, T and P the Rayleigh number R is increased until the lowest imaginary part of the eigenvalue ω becomes negative signalling the onset of convection. Table I indicates the rate of convergence with increasing truncation parameter for some typical examples. It is evident that usually $N_T=4$ is sufficient to approach the exact value to an accuracy of about 1%.

3. ONSET OF CONVECTION AT MODERATE PRANDTL NUMBERS

It is well known from earlier work (Roberts, 1968; Busse, 1970a; Gilman, 1975) on the onset of convection in rotating spheres or spherical shells that the inhibiting influence of the Coriolis force leads to an increasing critical wave number with increasing Taylor number τ^2 and to a time dependence in the form of a drift of the convection pattern relative to the rotating frame of reference. Only in the case of very thick shells with $\eta \lesssim 0.25$ does the onset of convection occur in the form of axisymmetric monotonously growing modes if the Prandtl number is sufficiently high and the Taylor number sufficiently low (Geiger and Busse, 1981). The present analysis confirms this picture for Prandtl numbers of the order unity or higher.

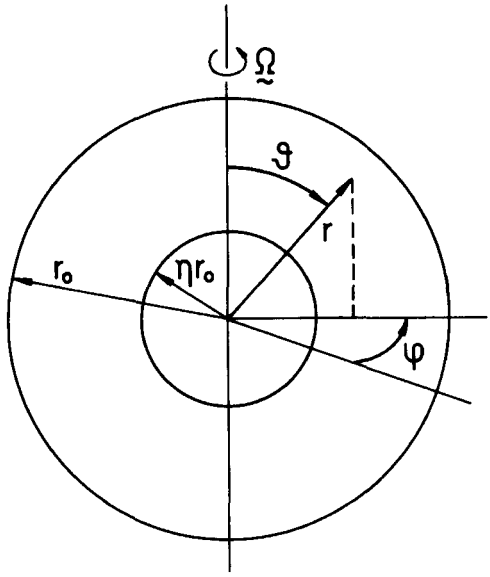

Figure 1 Geometrical configuration of the problem.

Figure 2a presents the critical Rayleigh number for different values of m as a function of the Taylor number at $P=10$. The corresponding values of the frequency ω are given in Figure 2b. Since the critical Rayleigh number increases with $T^{2/3}$ for asymptotically large T, $R/T^{2/3}$ has been plotted and the numerical results indicate the gradual approach to the asymptotic regime. At $T=10^7$ the critical Rayleigh number is still quite far from the asymptotic value $R_\infty \simeq 1.16\, T^{2/3}$, based on the value shown in Figure 3 of Busse (1970a). But there can be little doubt that an asymptotic law of this kind will be approached.

For the frequencies ω the asymptotic law of Busse (1970a) predicts $\omega_\infty \simeq 0.50 \cdot T^{-1/6} P^{-1}$ for $P \gtrsim 1$. The data given in Figure 2b show a tendency to approach this law. In the opposite limit the frequencies agree with analytical expressions of the low Taylor number case (Busse, 1973; Geiger and Busse, 1981),

$$\omega = 2(m+1)^{-1}(1+P\rho_l)^{-1} \tag{3.1}$$

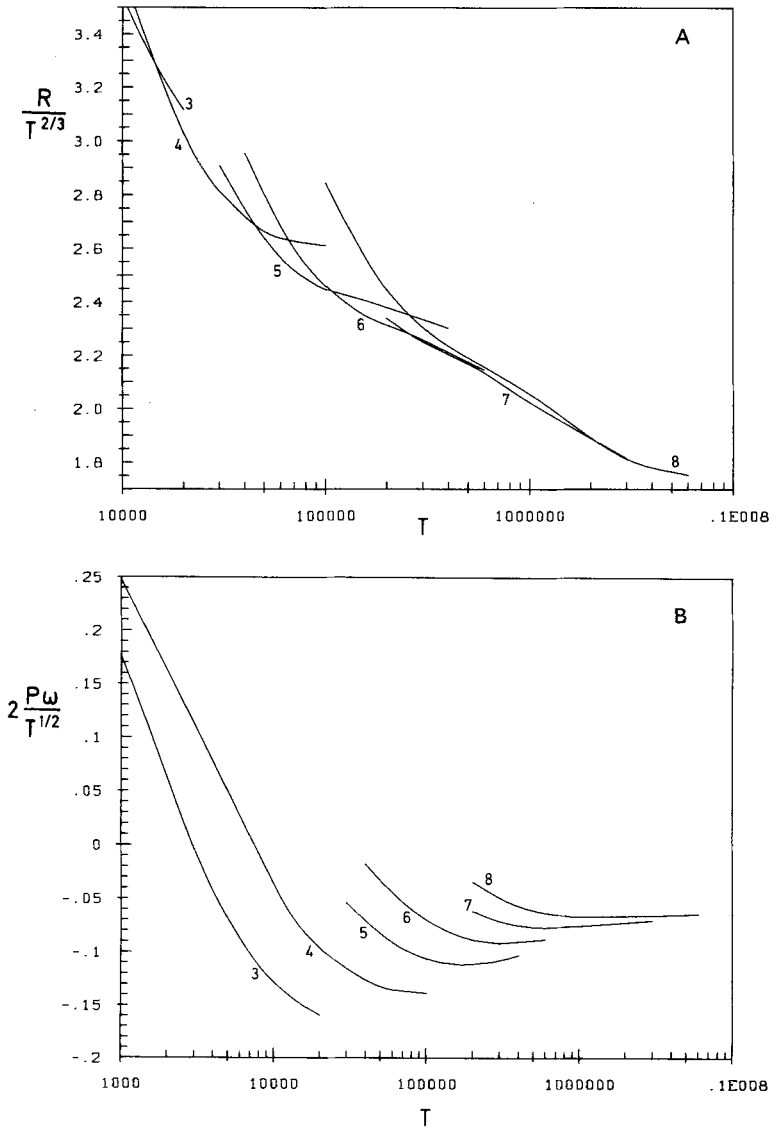

Figure 2 (A) Rayleigh numbers $R(T,m)$ for the onset of convection as a function of T are shown in Figure (A) for $P=10$ and $\eta=0.4$. The numbers indicate the value of m. (B) The frequencies $\omega(T,m)$ corresponding to the curves shown in Figure 2(A).

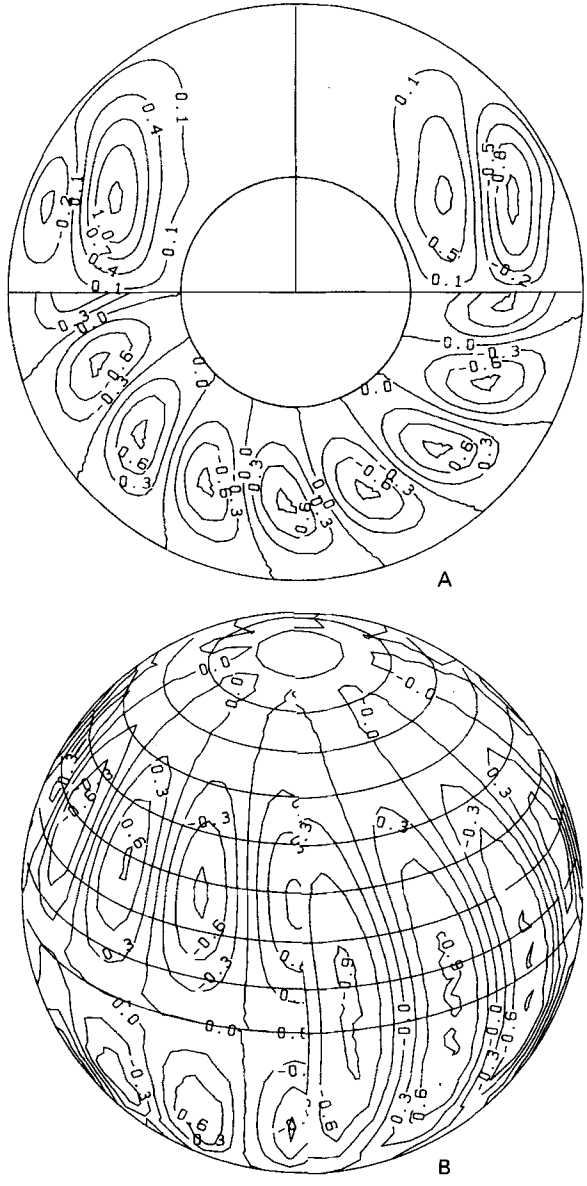

Figure 3 (A) Meridional and equatorial streamlines (F_ϕ=const. at $\phi=0,\pi/8$, F_θ=const. for $\pi\leqq\phi\leqq2\pi$) for $m=8$, $T=6\cdot10^6$, $R=57900$, $c=0.976$, $P=10$, $\eta=0.4$. (B) Streamlines (F_r=const.) on the left hemisphere and lines of constant radial velocity u_r on the right hemisphere at $r=1+\eta/2(1-\eta)$ for the same parameter values as in (A).

where ρ_t is approximately 0.95. The tendency of the convection motion to form columns aligned with the axis of rotation is shown in Figure 3 which indicates the streamline pattern relative to the drifting frame of reference, but without the mean zonal flow in the form of a rigid rotation corresponding to this frame of reference. For these plots we use the property that the velocity field (2.5) can be represented by the superposition three stream functions which describe streamlines on the meridional planes, the cones of constant latitude and the spherical surface of constant radius,

$$\mathbf{u}=\begin{bmatrix} -\dfrac{1}{r^2\sin\theta}\dfrac{\partial}{\partial\theta}F_\theta \\ \dfrac{1}{r\sin\theta}\dfrac{\partial}{\partial r}F_\theta \\ 0 \end{bmatrix}+\begin{bmatrix} -\dfrac{1}{r^2\sin\theta}\dfrac{\partial}{\partial\phi}F_\phi \\ 0 \\ \dfrac{1}{r}\dfrac{\partial}{\partial r}F_\phi \end{bmatrix}+\begin{bmatrix} 0 \\ \dfrac{1}{\sin\theta}\dfrac{\partial}{\partial\phi}F_r \\ -\dfrac{\partial}{\partial\theta}F_r \end{bmatrix} \tag{3.2a}$$

where the three stream functions are given by

$$F_\phi\equiv r\sin\theta\frac{\partial}{\partial\theta}v,\ F_\theta\equiv\frac{r}{\sin\theta}\frac{\partial}{\partial\phi}v,\ F_r\equiv w \tag{3.2b}$$

Lines of constant values of the functions F_θ, F_ϕ, and F_r have been plotted on meridional planes, on the equatorial plane and on the spherical surface $r=\frac{1}{2}(1+\eta)/(1-\eta)$, respectively. In addition lines of constant $L_2 v$ on that surface are shown on the right hemisphere of Figure 3(B). The tendency towards alignment with the axis of rotation is most evident in the meridional planes of Figure 3(A). The meridional planes are chosen rather arbitrarily at $\phi=0$ and at $\phi=\pi/2m$ in order to show some typical examples. The phase of the solution is determined in all cases by setting the coefficient a_{11m} equal to unity.

In all cases that have been investigated the lowest value of the Rayleigh number corresponds to the mode for which u_r and Θ are symmetric functions with respect to the equator. This property agrees with the finding (Busse, 1970b, 1973) that the mode described by the tesseral spherical harmonic $P_l^l e^{il\phi}$ is preferred among all spherical harmonics of the order l in a thin spherical shell in the

limit of low rotation rates. Only for thick shells with $\eta < 0.25$ exceptions from this rule appear to be possible (Geiger and Busse, 1981) as has already been mentioned above.

At $P = 1$, the critical Rayleigh number and the corresponding frequency ω follow a similar dependence on m as in the case $P = 10$. The curvature in the dependence on T of the critical Rayleigh number $R(T, m)$ for a given m does not change monotonously, however, as can be seen in Figure 4(A). This property gives rise to the surprising phenomena that $R(T, 4)$ is lower than $R(T, 2)$ around $T \simeq 700$ and again for $T \gtrsim 7 \cdot 10^4$. This non-monotonous dependence of R on m was unexpected and has stimulated the more detailed investigation at lower Prandtl number where this feature is even more pronounced.

The results shown in Figure 4 exhibit well the limit of low rotation rate. The Rayleigh number approaches the value calculated by Chandrasekhar (1961) in the non-rotating case, if the different normalization is taken into account, and the frequencies ω obey the relationship (3.1).

4. ONSET OF CONVECTION AT LOW PRANDTL NUMBERS

While for a given value of m the lowest Rayleigh number is a continuously differentiable function of T for Prandtl numbers of the order unity or higher, this property no longer holds when we proceed to lower Prandtl numbers. As is shown in Figure 5(A) for $P = 0.5$ two curves corresponding to two different modes with $m = 2$ intersect and the Rayleigh number for the onset of modes with $m = 2$ exhibits a kink. For comparison the mode $m = 2$ with antisymmetric functions u_r, Θ with respect to the equatorial plane is also shown. This mode exhibits the characteristic bend, but the "switch-over" has not yet happened. It will occur as P is decreased further.

The way in which this switch-over phenomenon occurs as a function of the Prandtl number is more clearly seen in Figure 6 where the same phenomenon is shown for $m = 6$ at somewhat lower Prandtl number. The original mode and a new mode which does not exist for $T = 0$ approach each other in R as well as in ω. At a certain Prandtl number P_s, $0.15 < P_s < 0.2$, a saddle point like singularity is

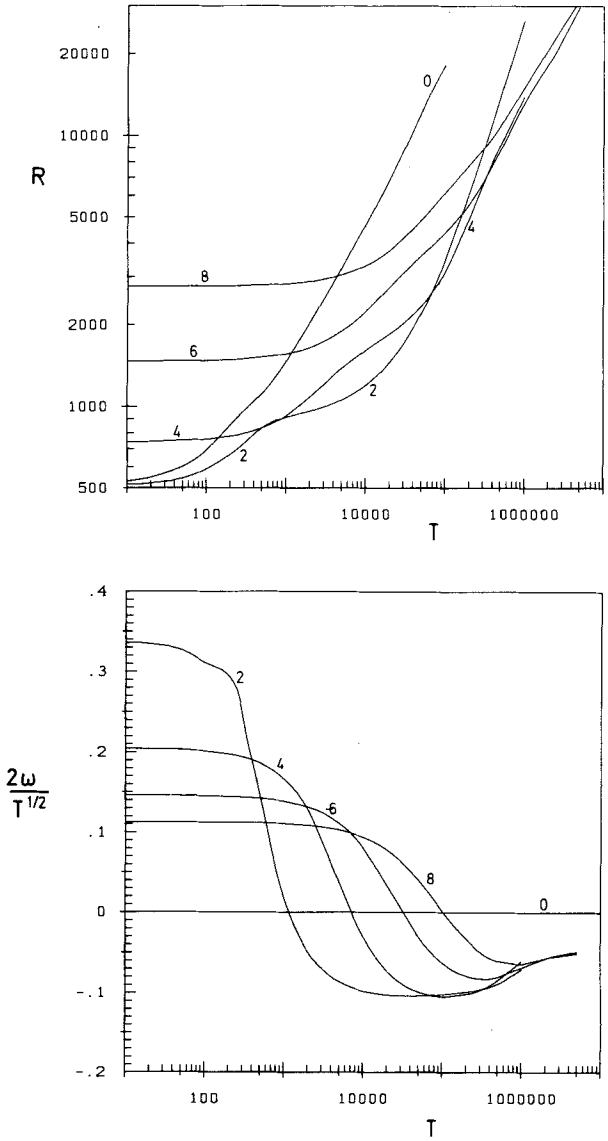

Figure 4 Rayleigh numbers $R(T,m)$, above, and frequencies $\omega(T,m)$, below at the onset of convection as a function of T are shown for $P=1$ and $\eta=0.4$. The numbers give the values of m.

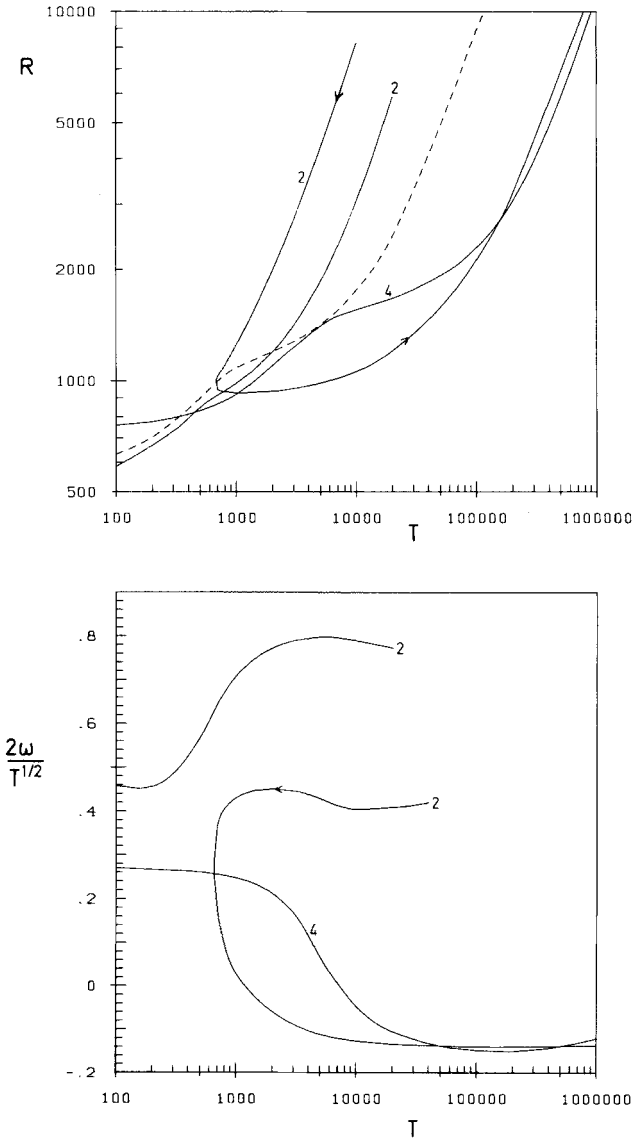

Figure 5 Rayleigh numbers $R(T,m)$, above, and frequencies $\omega(T,m)$, below, as a function of T for $P=0.5$ and $\eta=0.4$. The numbers indicate the value of m. The dashed line refers to the $m=2$ mode with an eigenfunction Θ which is antisymmetric with respect to the equatorial plane. In the upper figure the region of positive growth rates lies to the left of the arrows.

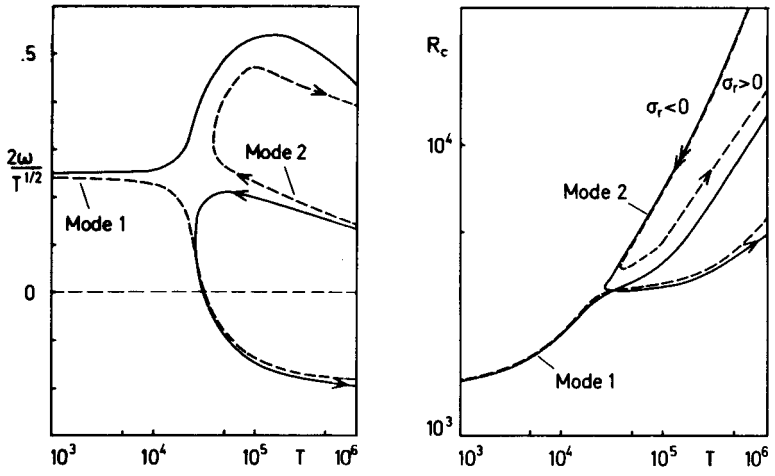

Figure 6 The "switch-over" phenomenon in the case $m=6$, $\eta=0.5$. Rayleigh numbers $R(T,6)$ are shown on the right side, the frequencies are given in the left figure. Dashed lines correspond to $P=0.2$, solid lines to $P=0.15$.

reached and below this Prandtl number the branches are connected in the opposite way. The attraction towards the singularity in the parameter space is responsible for the bends in the Rayleigh–Taylor number plots and gives rise to property that the mode with $m=4$ exhibits a lower Rayleigh number than the $m=2$ modes for $T\simeq 10^3$ as well as for $T\gtrsim 2\cdot 10^5$ as seen in Figure 5(A). At $P=0.1$ the switch-over has occurred for all m up to $m=6$ as is evident from Figure 7 except for the antisymmetric mode $m=6$.

The switch-over phenomenon typically occurs in eigenvalue problems which are not of the Sturm–Liouville type. Related example can be seen in Figure 5 of Busse and Or (1986) and a detailed discussion of the phenomenon has recently been given by Jones (1987). In the present case the switch-over occurs for all m that have been investigated at a Prandtl number P_s that decreases with increasing m. The corresponding changes in the eigenfunctions can be noticed in Figure 8. The preferred convection mode for low Taylor numbers is characterized by a positive ω and relatively small toroidal component of motion which vanishes in the limit $T\to 0$. The new mode entering the picture beyond a certain critical Taylor number exhibits properties of inertial modes in that the frequency ω

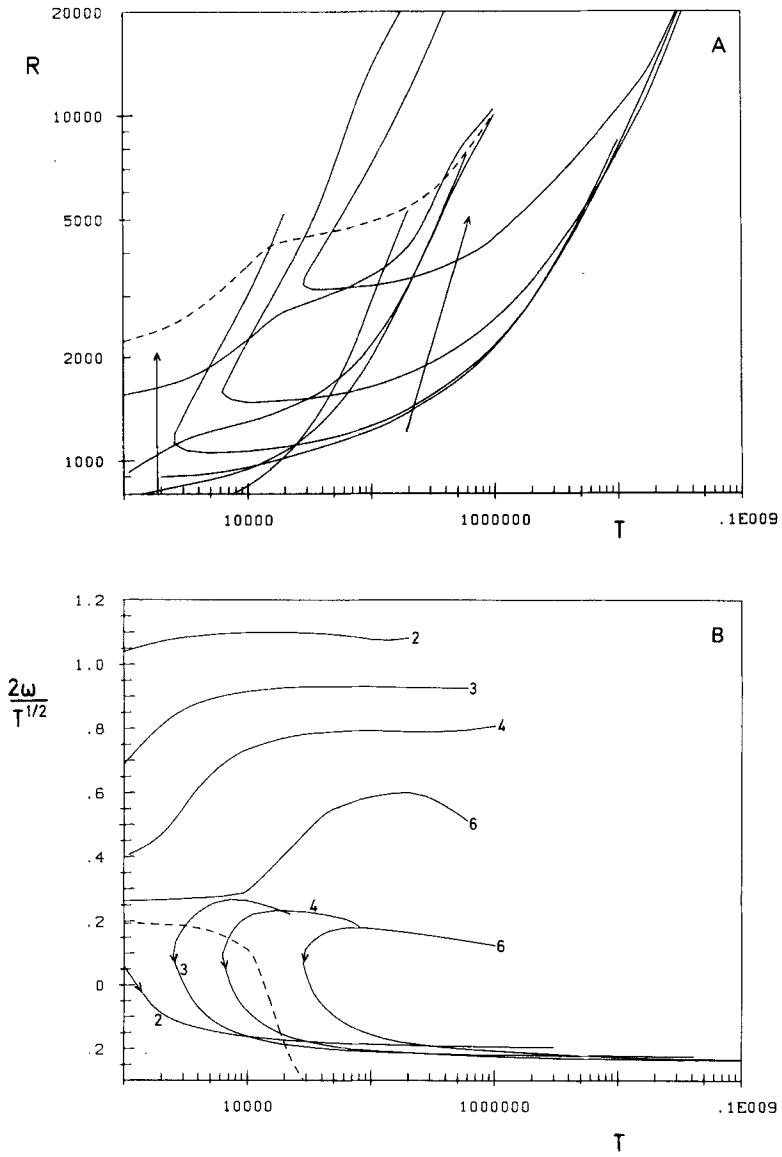

Figure 7 (A) Rayleigh numbers $R(T, m)$ for the onset of convection as a function of T for $P=0.1$, $\eta=0.4$. The curves in the direction of the arrows correspond to $m=2$, 3, 4, 6, respectively. The dashed curve indicates the odd mode $m=6$. (B) The frequencies $\omega(T, m)$ corresponding to the curves shown in Figure 7(A).

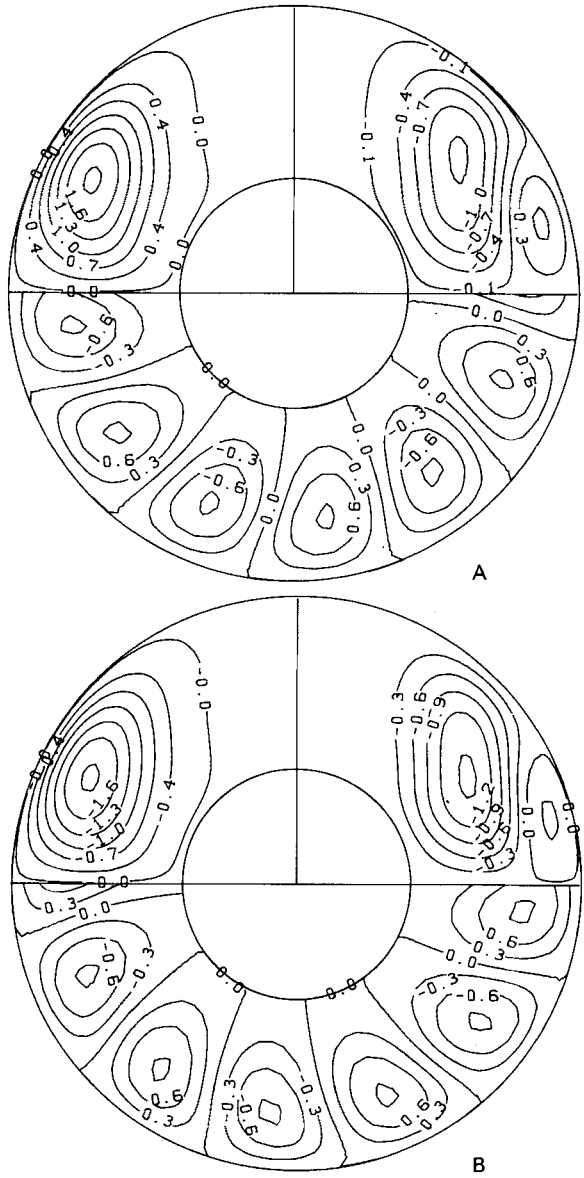

Figure 8 Meridional (F_ϕ=const. at $\phi=0$ on the right side and $\phi=\pi/12$ on the left side) and equatorial (F_θ=const.) streamlines for the mode evolving from $T=0$ (Figure A: $T=6\cdot10^4$, $R=3130$) and for the inertial wave mode (Figure B: $T=10^5$, $R=3200$); $P=0.1$, $\eta=0.4$ in both cases.

becomes independent of T as T increases and in that the toroidal component of motion plays a dominant role. Of the two branches which meet at the critical Taylor number only the branch with a negative ω is of interest because of its relatively low Rayleigh number. Its phase tends to increase with increasing distance from the axis as shown in Figure 8(B). This property is similar to that of the thermal Rossby waves which are preferred in the limit of asymptotically large values of T. An outward transport of angular momentum in the prograde direction is associated with this variation of the phase as will be discussed in more detail in Section 5. In contrast the phase of the low Taylor number mode decreases with increasing distance from the axis as is evident from Figure 8(A). The typical differences between the two modes are still noticeable at Prandtl numbers above P_s where there is a continuous change from one to the other. The change of the sign of ω indicates the transition region where the change in the properties occurs most rapidly.

The switch-over phenomenon appears to occur for all values of η at a Prandtl number somewhat above 0.1. Figure 9 demonstrates the phenomenon for $\eta = 0.8$ in which case $m = 10$ represents the preferred mode for low Taylor numbers. Again, a slight bend is noticeable in dependences of R and ω on T for $P = 1$, while a kink in the $R(T, 10)$ relationship and a corresponding jump in ω occur for $P = 0.1$.

The switch-over phenomenon which we have just discussed is not the only transition from one mode to another with the same symmetry that is observed at low Prandtl numbers. A second kind of transition develops at higher Taylor numbers of the order 10^8 as shown in Figure 10. Again the Rayleigh number curves of two modes with the same m intersect and the frequency ω of the preferred mode jumps by a finite amount at the point where the critical Rayleigh number exhibits a kink. The origin of this transition can be traced to the development of a loop in the R–T-relationship as demonstrated in Figure 11. For $P = 0.3$ there exist a smooth dependence $R(T, 6)$ albeit with a strong bend at $T = 1 \cdot 10^6$. But at $P = 0.25$ a loop has developed at the position of the bend. This loop expands rapidly with decreasing Prandtl number as is evident from the comparison with the case $P = 0.245$. For $P = 0.23$ the upper part of the loop has moved to very large Rayleigh numbers at which numerically reliable solutions could no longer be obtained. The formation of the loop corresponds to the appearance of a fold in the

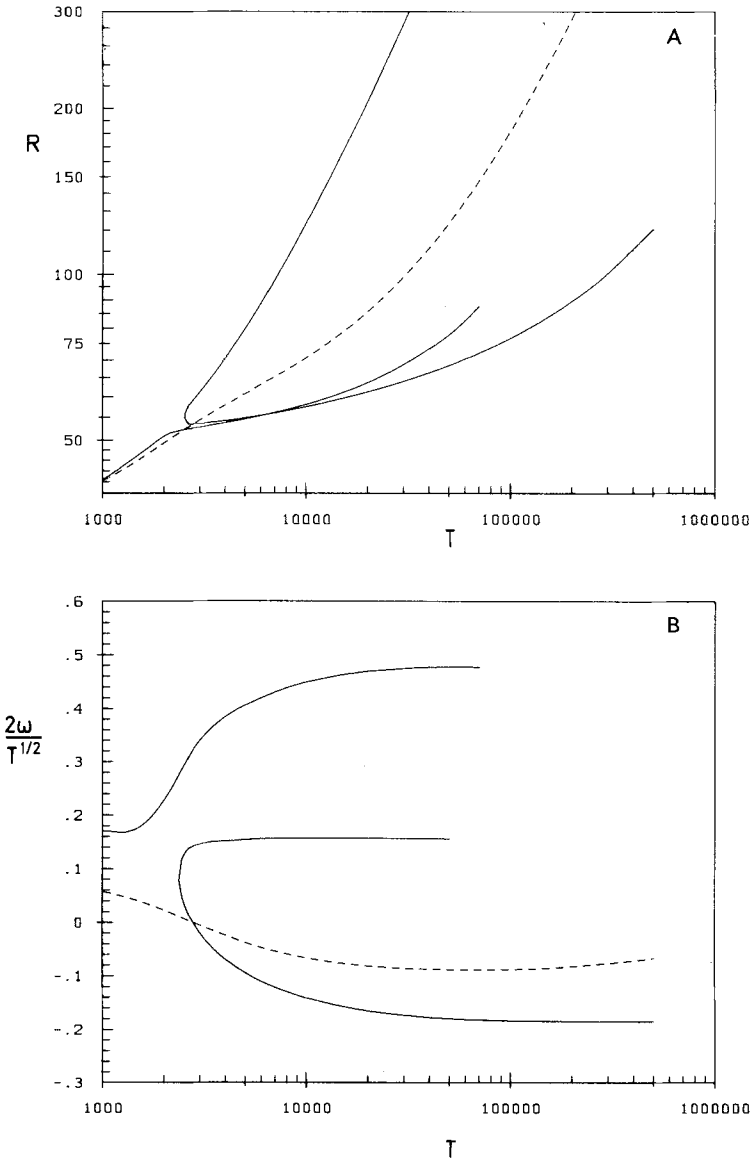

Figure 9 The "switch-over" phenomenon in the case $m=10$, $\eta=0.8$. $R(T,10)$ and $\omega(T,10)$ are shown in (A) and (B), respectively. Dashed lines refer to $P=1$, solid lines to $P=0.1$.

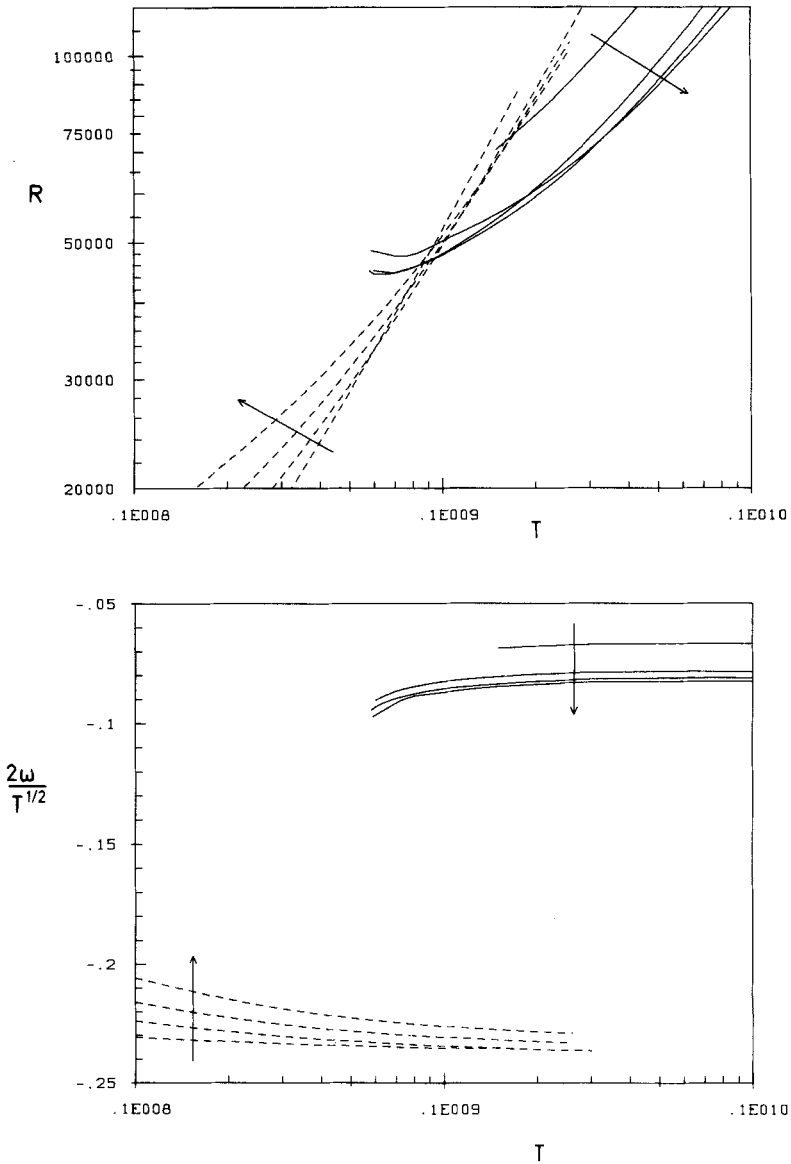

Figure 10 Rayleigh numbers $R(T,m)$ and frequencies $\omega(T,m)$ for $P=0.1$, $\eta=0.4$. The sequence of curves in the direction of the arrow is given by $m=4$, $m=6$, $m=7$, $m=8$. The dashed lines correspond to the fast drifting mode describing wall-attached convection, while the solid lines represent the columnar mode.

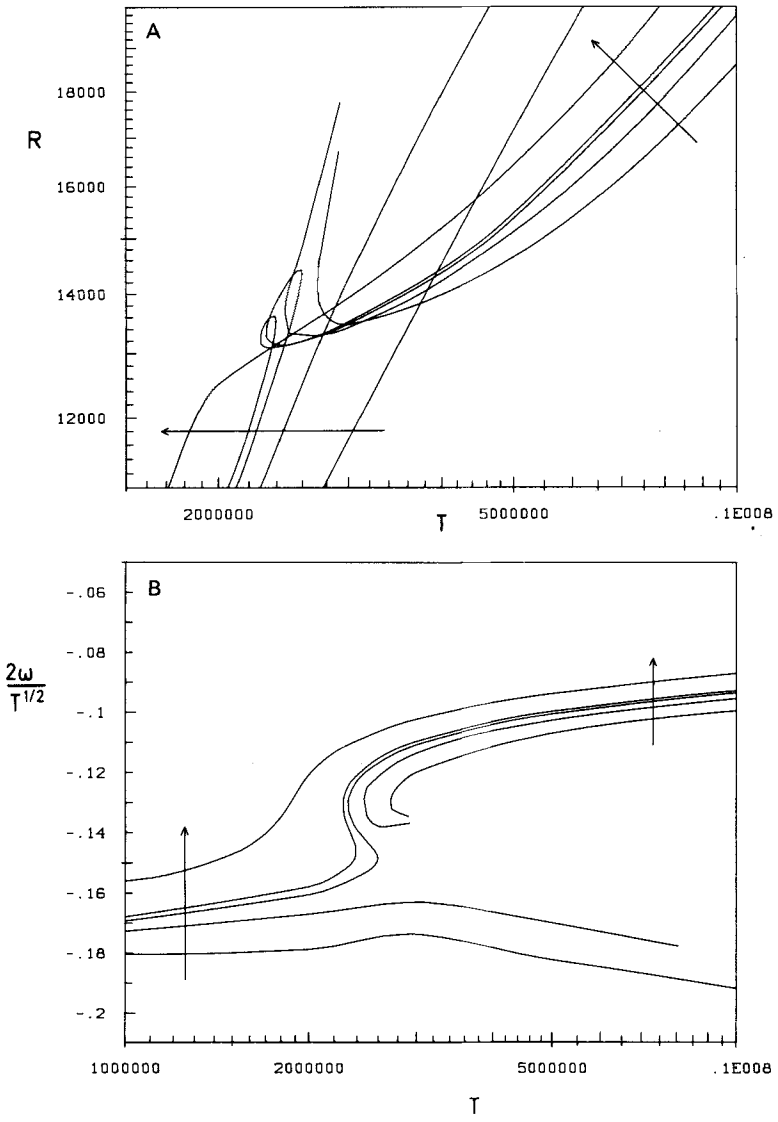

Figure 11 (A) Rayleigh numbers $R(T, 6)$ for $\eta = 0.4$ and for various Prandtl numbers. The sequence of curve in the direction of the arrow correspond to $P = 0.2$, 0.23, 0.245, 0.25, 0.3. (B) Frequencies $\omega(T, 6)$ corresponding to the curves of Figure 11(A).

ω–T-relationship. All jumps in the frequencies of Figure 10 are caused by S-shaped folds, but the lines connecting upper and lower branches have not been computed. There can be no doubt, however, that the S-shaped folds developed in all cases as indicated for $m=6$ in Figure 11(B).

The development of the S-shaped fold in the ω–T-relationship and the corresponding loop in the R–T-plane is associated with a typical change in the convection motion as shown in Figures 12 and 13. Below the transition Taylor number the convection eddies move outwards with increasing Taylor number and become attached to the equatorial region of the outer spherical boundary as shown in Figure 10. Beyond the transition the convection motions approach the form of columns aligned with the axis of rotation as predicted by the asymptotic theory (Busse, 1970). Because of the presence of the inner sphere and because of their finite thickness the columns are located at a somewhat larger distance from the axis than the distance of half the outer radius given by the asymptotic expressions.

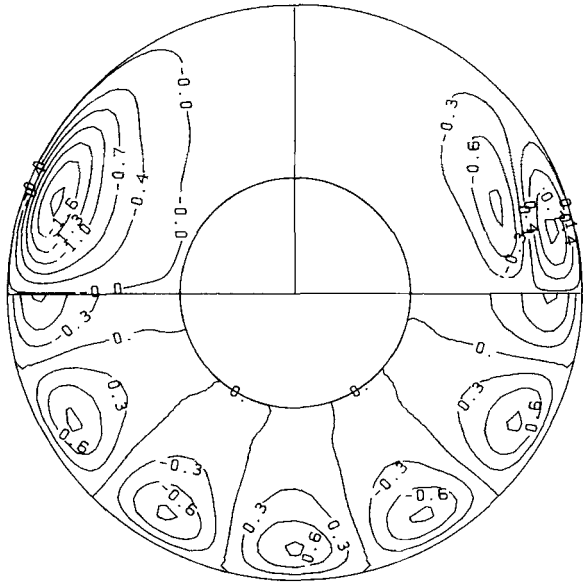

Figure 12 Meridional and equatorial streamlines (F_ϕ=const., at $\phi=0$, right and $\phi=\pi/12$, left, F_θ=const. in the lower half) for $m=6$, $T=9\cdot10^7$, $R=4.55\cdot10^4$, $c=185$, $P=0.1$, $\eta=0.4$.

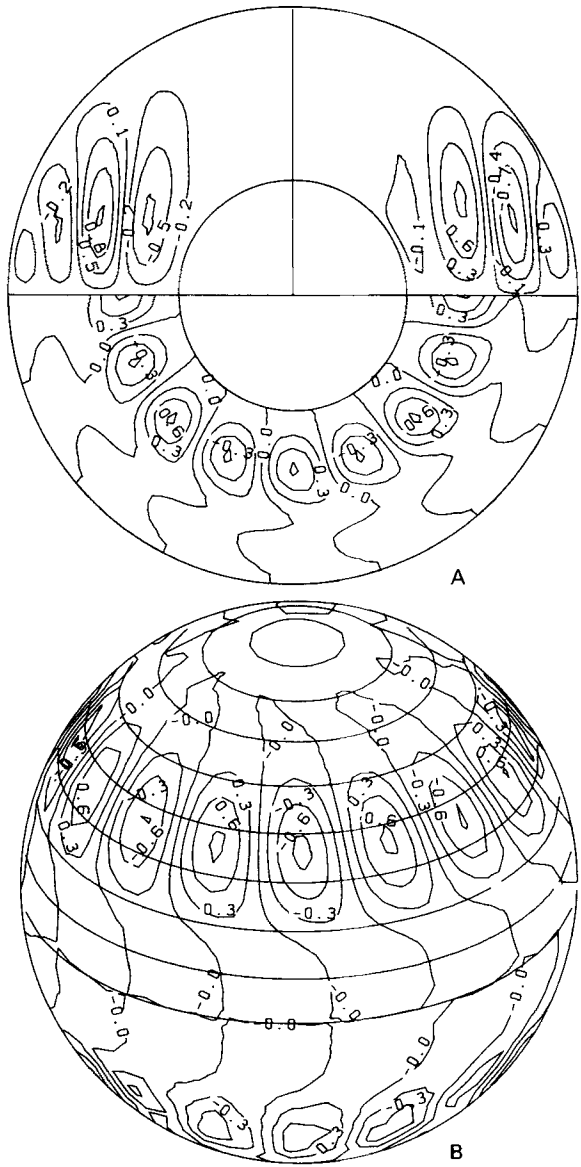

Figure 13 (A) Meridional and equatorial streamlines (F_ϕ=const., at $\phi=0$, right, and $\phi=\pi/16$, left; F_θ=const. in the lower half) for $m=8$, $T=10^9$, $R=1.34\cdot10^5$, $c=119$, $P=0.1$, $\eta=0.4$. (B) Lines of constant radial velocity at $r=1+\eta/2(1-\eta)$ for the same parameter values as (A).

Figure 13(A) also shows a significant variation of the phase with distance from the axis at least in the neighborhood of the column. Such a variation had become almost negligible with increasing Taylor number for the mode attached to the outer boundary. Accordingly we expect a strong outward transport of momentum as soon as the columnar mode grows to a finite amplitude.

5. NONLINEAR PROPERTIES OF CONVECTION

Only some typical examples of nonlinear properties will be presented in this section. A comprehensive description of the dependences on all external parameters of the problem would go far beyond the scope of this paper. Some additional results will be given in a future paper (Zhang and Busse, 1987) which will also include results on the stability of nonlinear convection solutions.

The convection mode which is preferred at low Taylor numbers exhibits the features to be expected on the basis of the small amplitude perturbation theory for a thin shell (Busse 1970b, 1973). The differential rotation shown in Figure 14(A) exhibits a complex structure owing to the competing effects of the azimuthal Reynolds stress and of the momentum advection by the axisymmetric meridional circulation as shown in Figure 14(B). In comparing the

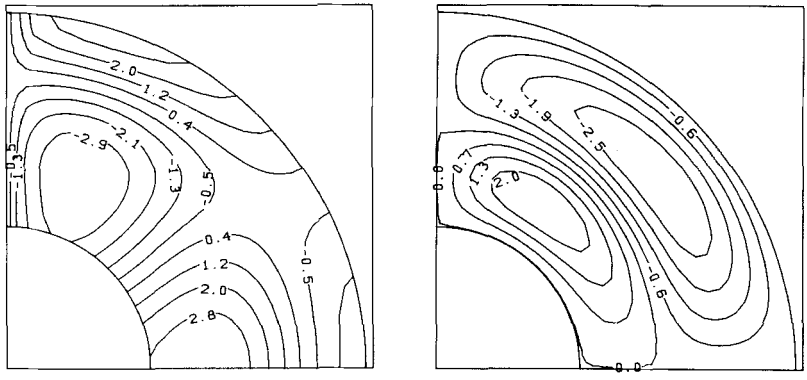

Figure 14 Lines of constant differential rotation (left) and streamlines of the axisymmetric meridional circulation (right) for convection with ($m=2$)-periodicity at $T=10^4$, $R=892=R_c+46.5$, $P=0.1$ (positive-ω-mode).

present results with those of other papers it should be kept in mind that the solution has been normalized by setting $c_{011}=0$, i.e., the rigid rotation component of the solution is the same as in the static state. The angular momentum on the other hand will in general differ from that of the static state. The meridional circulation exhibits the typical double-cell structure which is caused by the fact that the interior of the fluid shell becomes more isothermal in the equatorial region than in the polar region owing to the efficiency of equatorial convection. As a result the outer circulation rises at the equator and descends at high latitude while the opposite direction characterizes the lower cell. At the low Prandtl number of Figure 14(B) the latitudinal inhomogeneity in the advection of radial and latitudinal momentum is actually the dominant contributor to the meridional circulation. But the effect remains the same.

The nonlinear properties change somewhat after the onset of the mode with negative ω. In this case the azimuthal Reynolds stress caused by the increasing phase of the fluctuating component with distance from the axis is the dominant effect in establishing the differential rotation shown in Figure 15(A). The zonal flow in the prograde direction increases with distance from the axis and the surfaces of constant differential rotation approach the cylindrical form characteristic for high Taylor numbers. Figure 15(B) shows that the outer meridional circulation cell has displaced the inner one

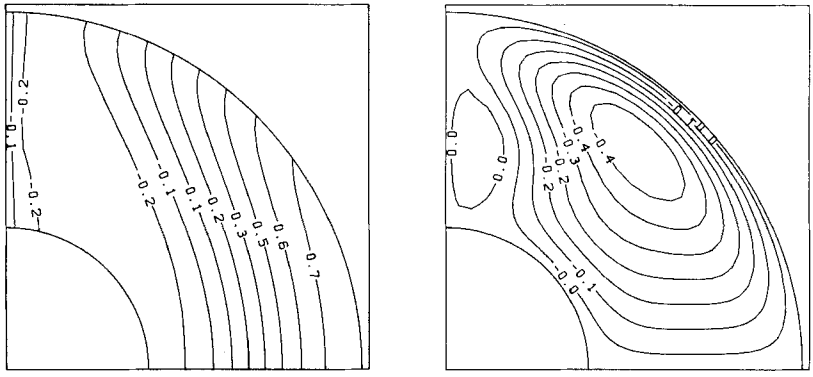

Figure 15 Lines of constant differential rotation (left) and streamlines of the axisymmetric meridional circulation (right) for convection with ($m=2$)-periodicity at $T=10^5$, $R=1300=R_c+46.3$, $P=0.1$ (negative-ω-mode).

almost entirely. As the Taylor number increases, the amplitude of the meridional circulation decreases in comparison to the other components of motion.

Figure 16 depicts the latitudinal variation of the convective heat transport. The positive-ω-mode exhibits a maximum of the heat transport at the equator both at the inner and at the outer boundary. The property that the additional heat transport owing to convection is negative at higher latitudes is caused by the meridional circulation. Since the meridional circulation moves away from both boundaries at higher latitudes it tends to decrease the absolute value of the temperature gradient at the boundaries. The negative-ω-mode exhibits somewhat different properties. Since there is essentially only one meridional circulation cell left, we encounter the phenomenon of decreased heat transport only at the outer boundary of the polar

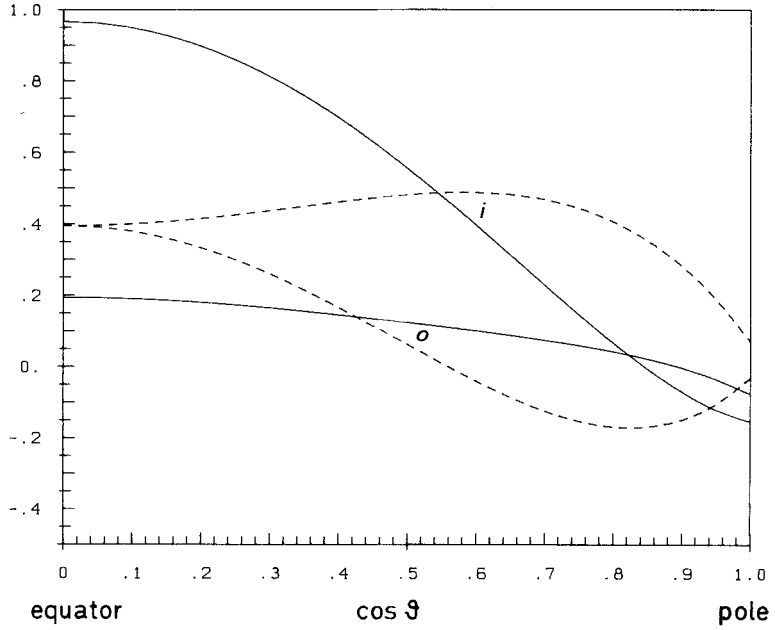

Figure 16 The convective heat transport as a function of the latitude ($\theta = \arccos x =$ colatitude) for the positive-ω-mode ($T = 10^4$, $R = 892$, $P = 0.1$, solid lines) and for the negative-ω-mode ($T = 10^5$, $R = 1300$, $P = 0.1$, dashed lines, amplitude multiplied by 20). $-\partial\bar{\Theta}/\partial r$ has been plotted at the inner (i) and outer (o) boundaries, where $\bar{\Theta}$ denotes the $(m = 0)$-component of Θ.

region. The main difference between the two modes is the much lower mean value of the heat transport by the negative-ω-mode. A closer inspection of the Nusselt number dependence shows that the positive-ω-mode exhibits a subcritical finite amplitude onset at the low Prandtl number of 0.1, while the negative-ω-mode does not show this phenomenon. At higher Prandtl numbers the amplitudes of the two approach each other at the same value of $(R-R_c)/R_c$.

6. DISCUSSION

The main result of the research reported in this paper is the observation of jumps in the structure of modes describing the onset of convection as function of the Taylor number even when the azimuthal wavenumber m is fixed. In Figure 17 the approximate transitions in the structure of solutions are indicated. The value of m is always determined by the critical Rayleigh number for the

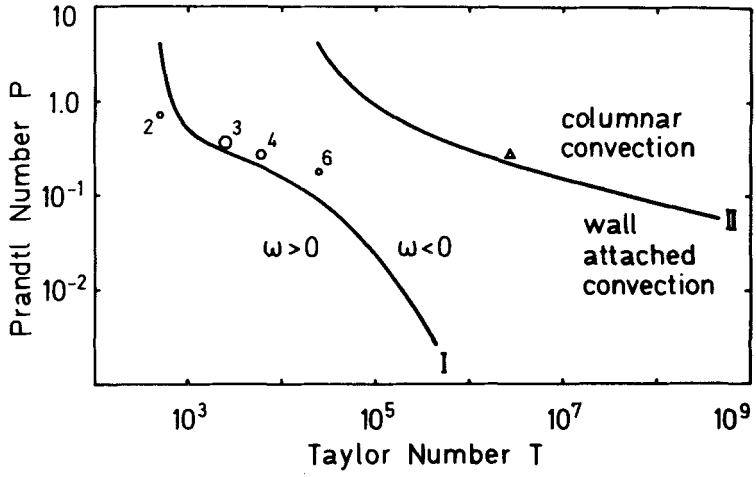

Figure 17 Regimes of different kind of modes in the Prandtl number–Taylor number plane. In the region to left of line *I* modes with positive ω (retrograde phase velocity) are preferred while towards the right modes with a positive phase velocity are preferred. In the neighborhood of the left side of line *II* the wall-attached mode is preferred while to the right of line *II* the columnar mode is preferred. The circles indicate the point at which the switch-over transition occurs for different values of m. The triangle indicates the point of loop formation for $m=6$.

corresponding values of T and P. As we have already mentioned, the point at which a discontinuity between the positive-ω-mode and the negative-ω-mode develops is nearly independent of the Prandtl number. The point at which the second kind of discontinuity in the form of a loop develops has not been well determined, but it seems to develop for all m in the neighborhood of the point which has been determined for $m=6$ as indicated in the figure. The position of the bend and the kink in the critical Rayleigh number relationship $R_c(T)$ for higher and lower Prandtl number, respectively, can be determined fairly well as shown by the line II in the Figure. The slope of this line suggests that the wall-attached mode may represent the preferred form of convection in the case of asymptotic high Taylor numbers if the limit is approached such that $TP^n=$const. with a positive n less than a critical value n_c which appears to be about 4.

The fact that the discontinuities develop as the Prandtl number decreases indicates the important role played by the limit of vanishing Prandtl number. It is well known (see, for example, Soward, 1977) that convection in a rapidly rotating sphere can be described as a perturbation of inertial waves with the Prandtl number as small parameters. The transition from the mode dominated by dissipation to the inertial mode corresponds to line I in Figure 17. The usual asymptotic theory appears to apply to the columnar mode which is preferred in the region beyond the line II of the diagram. The question whether convection in the intermediate regime can be described analytically in the limit of low Prandtl number is open at this time. It is also not clear whether the slope of line II has asymptotic character. The increasing demands for high resolution at high Taylor numbers have prevented us to continue the investigation of the transition II to lower Prandtl numbers. Perhaps the competition between the wall-attached mode and the columnar mode is similar to the competition between two modes found numerically by Buell and Catton (1983). An asymptotic boundary layer theory for the latter problem appears to be feasible, but has not yet been done.

Acknowledgement

The research reported in this paper has been supported in part by the Earth Sciences Section of the U.S. National Science Foundation and by the Deutsche Forschungsgemeinschaft under Grant BU-589.

References

Buell, J. C. and Catton, I., "Effect of rotation on the stability of a bounded cylindrical layer of fluid heated from below," *Phys. Fluids* **26,** 892–996 (1983).

Busse, F. H., "Thermal instabilities in rapidly rotating systems," *J. Fluid Mech.* **44,** 441–460 (1970a).

Busse, F. H., "Differential rotation in stellar convection zones," *Astrophys. J.* **159,** 629–639 (1970b).

Busse, F. H., "Differential rotation in stellar convection zones II," *Astron. & Astrophys.* **28,** 27–37 (1973).

Busse, F. H. and Or, A. C., "Convection in a rotating cylindrical annulus: Thermal Rossby waves," *J. Fluid Mech.* **16,** 173–187 (1986).

Chandrasekhar, S., "Hydrodynamic and hydromagnetic stability," Clarendon Press, Oxford (1961).

Cuong, P. G., "Thermal convection and magnetic field generation in rotating spherical shells," Dissertation, University of California, Los Angeles (1979).

Geiger, G. and Busse, F. H., "On the onset of thermal convection in slowly rotating fluid shells," *Geophys. Astrophys. Fluid Dynamics* **18,** 147–156 (1981).

Gilman, P. A., "Linear simulations of Boussinesq convection in a deep rotating spherical shell," *J. Atmos. Sci.* **32,** 1331–1352 (1975).

Jones, C. A., "Multiple Eigenvalues and mode classification in Plane Poiseuille Flow," *Quart. J. Mech. Appl. Math.*, to be published (1987).

Roberts, P. H., "On the thermal instability of a highly rotating fluid sphere," *Astrophys. J.* **141,** 240–250 (1965).

Roberts, P. H., "On the thermal instability of a rotating-fluid sphere containing heat sources," *Phil. Trans. R. Soc. London A.* **263,** 93–117 (1968).

Soward, A. M., "On the finite amplitude thermal instability in a rapidly rotating fluid sphere," *Geophys. & Astrophys. Fluid Dyn.* **9,** 19–74 (1977).